Continental Shelf Research 258 (2023) 104985

Contents lists available at ScienceDirect

Continental Shelf Research

journal homepage: www.elsevier.com/locate/csr

Energy transfer from sub-inertial Kelvin waves to continental shelf waves at a transverse bottom escarpment

Jan Erik H. Weber [a,*], Pål Erik Isachsen [a,b]

[a] Department of Geosciences, University of Oslo, Oslo, Norway
[b] Norwegian Meteorological Institute, Oslo, Norway

ARTICLE INFO

Keywords:
Coastal Kelvin waves
Continental shelf waves
Energy transfer
Effect of transverse bottom escarpment

ABSTRACT

We consider barotropic coastally-trapped Kelvin waves of tidal origin along a straight coast that propagate from deeper water across a transverse bottom escarpment into a more shallow region. The M_2 component, which has a frequency above the inertial frequency f, is modified by crossing the escarpment, but continues basically as a Kelvin wave into the shallow region. For tidal components that have frequencies smaller than f, like K_1, some of the energy in the Kelvin wave is converted into a continental shelf wave (CSW) that follows the escarpment with shallow water to the right (in the northern hemisphere). The theory is applied to the shelf north-west of Norway where the deep Norwegian Sea is separated from the much shallower Barents Sea by an escarpment reaching from the north-Norwegian coast towards Spitsbergen. By introducing an idealized bottom topography and coastal geometry, analytical calculations and numerical modeling are used to investigate the energy flux in CSWs towards Spitsbergen caused by sub-inertial Kelvin wave motion along the west coast of Norway. Both analytical and numerical calculations indicate that the CSW energy flux towards Spitsbergen is about eighty percent of the incident sub-inertial Kelvin wave energy flux, and that only twenty percent of the energy flux is transmitted into the Barents Sea in the form of sub-inertial Kelvin waves.

1. Introduction

The barotropic tidal motion along a coastline manifests itself primarily as a Kelvin wave, propagating at the shallow-water phase speed with the coast to its right in the northern hemisphere. In the ideal flat-bottom ocean, the wave amplitude decays exponentially away from the coast at a scale set by the external Rossby radius of deformation. Even for realistic coastal geometries and bottom topographies, the Kelvin wave signature is often seen. Fig. 1 shows the sea surface height (SSH) amplitude of the major semi-diurnal (M_2) and diurnal (K_1) tides off the Norwegian coast as estimated by the TPXO (v9) tidal inversion analysis by Egbert and Erofeeva (2002). Indeed, both constituents propagate northeastward along the coast at speeds agreeing roughly with the shallow-water phase speed calculated from the continental shelf depth, and with amplitudes that decay approximately according to the corresponding Rossby radius.

The TPXO analysis nonetheless points to a qualitative difference in behavior around the Barents Sea Opening (BSO) north of about 70°N, where the Norwegian coastline turns eastward into the Barents Sea while the continental slope continues northward towards Spitsbergen (part of the Svalbard archipelago). The tidal inversion solution is noisy but suggests the presence of diurnal tidal energy along the continental slope towards Spitsbergen. Diurnal energy also appears to wrap around the island group. In contrast, energy along the BSO is conspicuously absent for the semi-diurnal tide. In fact, as seen from Fig. 1, the M_2 tide is moderate in the Norwegian Sea, except for energy trapping at the north-west coast of Norway.

Just south of 70°N, where the coast and continental slope diverge, the shelf is extremely narrow (approx. 20 km). Here, the tidal waves practically experience a deep ocean that runs into a near-vertical sub-surface wall. For a high-resolution model of the tides in this region, we refer to Moe et al. (2002). At the most basic level, a coastally trapped Kelvin wave experiences the subsequent diverging paths of the coastline and continental slope as a change in ocean depth (a transverse escarpment) as it propagates along the coastline into the Barents Sea. When a Kelvin wave crosses such an escarpment, propagating from deep to more shallow water, it becomes modified, i.e. the propagation speed is reduced and the amplitude is increased. However, it cannot be reflected (propagate in the opposite direction) since this would violate the cross-shore geostrophic balance condition. The M_2 component can

* Corresponding author.
E-mail addresses: j.e.weber@geo.uio.no (J.E.H. Weber), p.e.isachsen@geo.uio.no (P.E. Isachsen).

https://doi.org/10.1016/j.csr.2023.104985
Received 6 October 2022; Received in revised form 25 February 2023; Accepted 29 March 2023
Available online 1 April 2023

radiate some energy away from the coast in the form of Poincaré waves at these latitudes, but the diurnal K_1 component, being sub-inertial, cannot do so.

However, some of the diurnal tidal energy may be transferred to low-frequency continental shelf waves (CSWs) that can propagate along the escarpment. We refer to these waves as double Kelvin waves if the shallow and deep regions have infinite horizontal extent (Longuet-Higgins, 1968). The CSWs are basically governed by the conservation of potential vorticity. Relative vorticity is generated by stretching and compression as water columns are moved back and forth across the bottom contours, causing wave propagation with shallow water to the right in the northern hemisphere (Longuet-Higgins, 1965). Importantly, since CSWs generally have frequencies that are smaller than the inertial frequency (Huthnance, 1975), this kind of transfer can only occur for the diurnal (and longer) components of the tidal coastal Kelvin wave.

The idea that tidal diurnal motion can generate vorticity waves on continental shelves, are far from new. In particular, strong tidal currents through straits, moving fluid columns across the shelf slope, may generate such waves. Examples are Buchwald and Kachoyan (1987), Middleton (1988) and Morrow et al. (1990) for CSWs along the Australian shelf from tides in the Bass Strait, and Foreman and Thomson (1997) for CSW generation in the Juan de Fuca Strait; see also Weber and Børve (2021, 2022) for the tidally-driven Moskstraumen in north Norway. Even in cases without a strait, CSWs with diurnal frequency may be generated on the shelf slope if the local group velocity is close to zero due to changes in topography; see e.g. Cartwright (1969) for the shelf near St. Kilda in the UK and Lam (1999) for the Greenland shelf. However, the CSW generation problem considered here, when a tidal coastal Kelvin wave meets an abrupt change in ocean depth (an escarpment) normal to its propagation direction, has apparently not been studied before.

As a prelude to our study, we recapitulate the dispersion relation by Drivdal et al. (2016) (hereafter referred to as DWD) for CSWs at various locations along the north-Norwegian coast, using fitted exponential profiles for the topographic slopes. Their dispersion diagram for three locations is reproduced in Fig. 2, where red lines correspond to the Barents Sea Opening. It is evident from their calculation that a CSW with diurnal frequency ($\omega_{K_1}/f = 0.56$) is possible along the escarpment. The figure shows that the energy in a long wave propagates northward, while the energy in a much shorter wave may propagate southwards. The study of DWD did not, however, investigate the *sources* of CSW energy in this region.

As stated above, we hypothesize that the diurnal tidal energy observed along the Barents Sea Opening represents CSWs that are generated as the diurnal Kelvin wave traverses the sharp change in ocean depth in propagating into the shallow Barents Sea. The semi-diurnal tide, in contrast, is unable to form CSWs at these latitudes. We need only consider the first mode of the diurnal CSW, since the second (and higher) modes have too small frequencies for being generated by K_1; see the dispersion diagram in DWD, their Fig. 4.

The rest of this paper is structured as follows: Section 2 presents a mathematical analysis of small-amplitude CSWs along an escarpment with constant-depth shelves of finite widths on both sides. In Section 3, we consider the energy fluxes in coastally trapped Kelvin waves and CSWs, and solve for the latter by postulating an energy flux balance. Section 4 presents numerical simulations from the ROMS ocean model, configured in 2D mode, verifying the existence of CSWs along the escarpment. Finally, Section 5 contains a summary and some concluding remarks.

2. Mathematical analysis

To reveal the physics of the phenomena studied in this paper, we simplify the geometry of the ocean basin. We note from Fig. 1 that the bottom contours along the continental slope that separates the Norwegian Sea and the Barents Sea, are fairly straight and directed (almost) northwards. Close to the Norwegian coast, at around 70°N, the deep-water contours exhibit an approximate 90° turn. In contrast, the coast itself curves very gently into the Barents Sea. Hence, we choose an idealized geometry with a straight coast in the east-west direction, intersected by a northward-directed escarpment.

In Fig. 3, we display a sketch of the physics studied in this paper with a Kelvin wave propagating eastward along the coastal boundary. The deep ocean in the west is connected to a shallower ocean in the east via a bottom escarpment, and a possible CSW propagation along this escarpment is the focus of the following study. In our mathematical analysis of the trapped wave motion over the escarpment, we place the x-axis along the Norwegian coast, pointing eastwards. The y-axis is directed northwards towards Spitsbergen.

We further idealize the bottom topography across the escarpment along the lines of Buchwald and Adams (1968), using an exponential profile (as done by DWD). Fig. 4 shows this profile with region 1 denoting the deep Norwegian Sea, region 2 the escarpment and 3 the shallow Barents Sea. Specifically, the bottom profile has the form

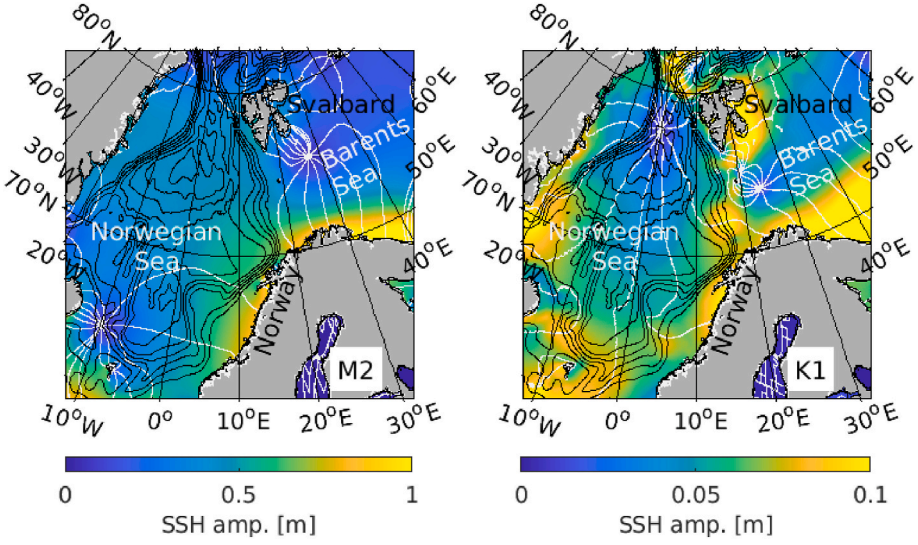

Fig. 1. The SSH amplitude of the M_2 (left) and K_1 (right) tide off the north-Norwegian coast, as estimated by the TPXO tidal inversion analysis. Co-tidal lines (white curves) are depicted for every hour (M_2) and every second hour (K_1).

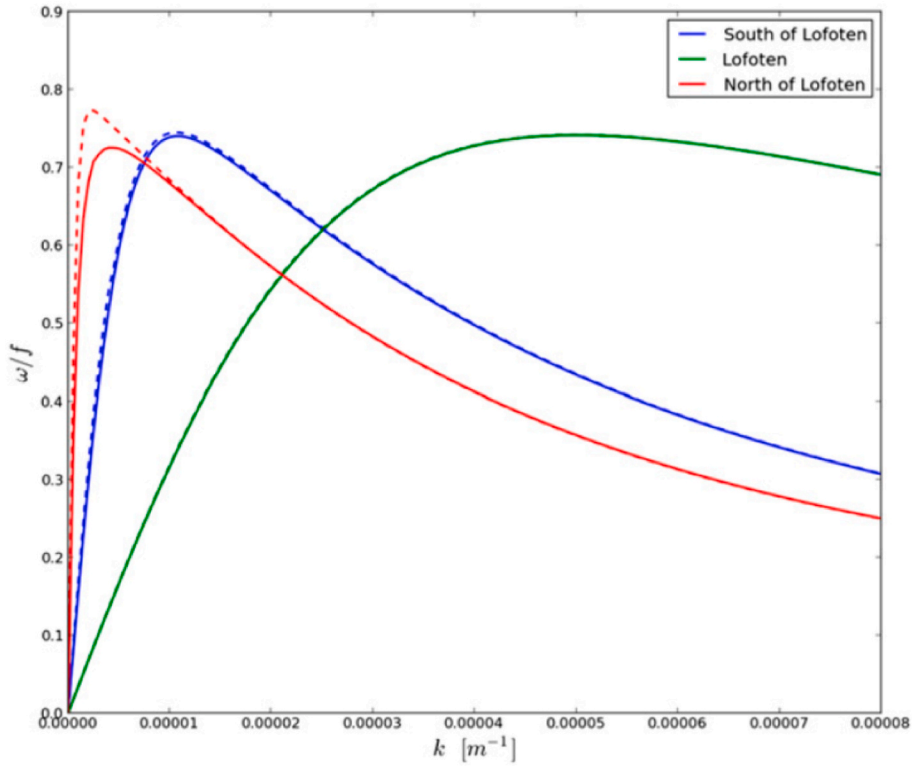

Fig. 2. CSW dispersion diagram (first mode) for three fitted exponential bottom profiles along the Norwegian coast. Here k is the wave number along the escarpment (which is denoted by l in the present study). The red line corresponds to conditions along the Barents Sea Opening. The dashed lines are calculated by using the rigid lid approximation. Adapted from DWD, their Fig. 5.

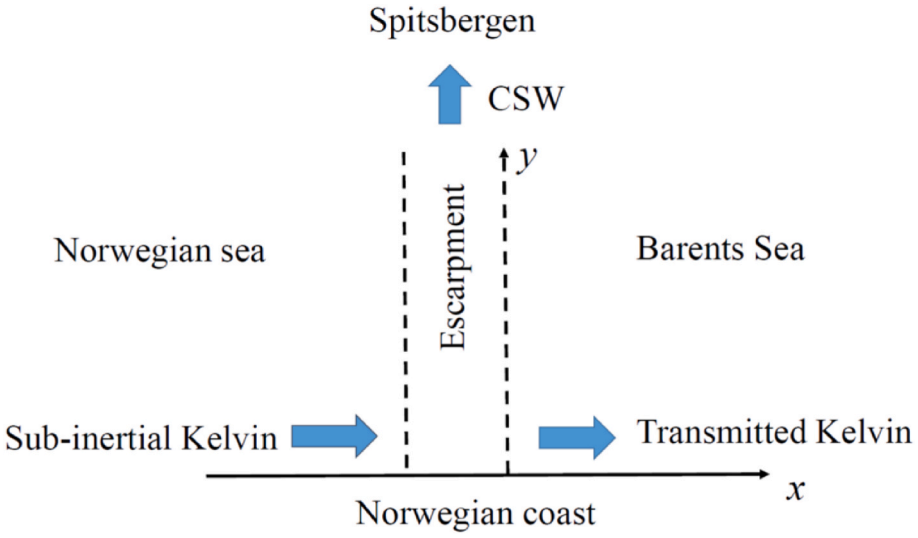

Fig. 3. Schematic picture of the physical situation: A tidally induced Kelvin wave with sub-inertial frequency meets the transverse escarpment towards Spitsbergen and generates a CSW, while a transmitted modified Kelvin wave continues along the coast into the shallow Barents Sea.

$$H = \begin{cases} H_1 = H_0 \exp(2bB), & -D_1 \le x \le -B \\ H_2 = H_0 \exp(-2bx), & -B \le x \le 0 \\ H_3 = H_0, & 0 \le x \le D_3. \end{cases} \tag{1}$$

Here, b is a constant describing the steepness of the slope while B is the width of the escarpment. From DWD we take $B = 100$ km, $b = 1.117 \times 10^{-5}$ m^{-1}, $H_0 = 300$ m, and $H_1 = 2800$ m. We return to the values of D_1 and D_3 later on.

The mathematical analysis of the CSWs follows closely that of DWD. However, we can simplify, because the rigid lid approximation works quite well for this problem, as shown in Fig. 2. The continuity equation then allows for the introduction of a stream function ψ such that $uH = -\psi_y$ and $vH = \psi_x$, where u and v are the velocity components in the x and y directions, respectively, and H is given by (1). We assume that the waves are so long that the pressure is hydrostatic in the vertical direction. The following analysis is standard, and we just give a short outline. Neglecting any effects of friction, the linear momentum equations in the regions $n = 1, 2, 3$ become (Buchwald and Adams, 1968; Gill and

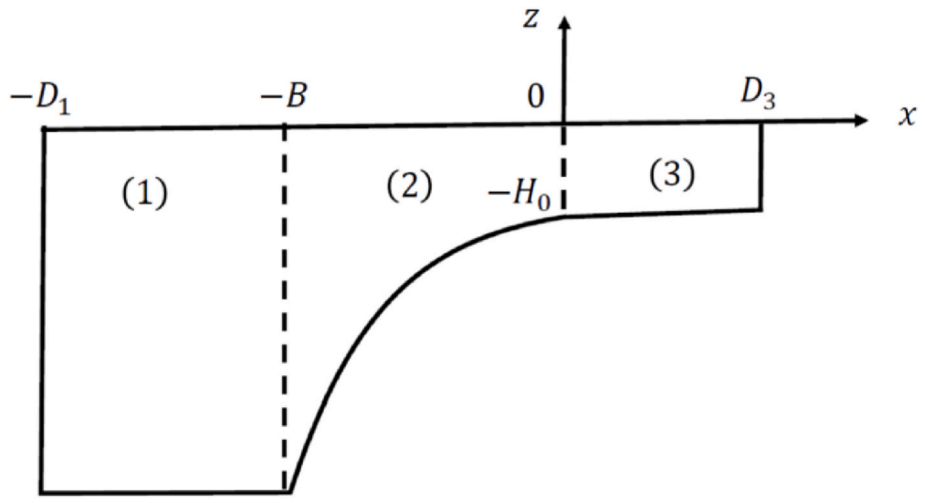

Fig. 4. A diagram of the idealized bottom topography in the Barents Sea Opening.

Schumann, 1974)

$$-\psi_{nty} - f\psi_{nx} = -gH_n\eta_{nx} \tag{2}$$

$$\psi_{ntx} - f\psi_{ny} = -gH_n\eta_{ny} \tag{3}$$

where η is the surface elevation. Furthermore, f is the constant Coriolis parameter, and g is the acceleration due to gravity. We now introduce a travelling wave solution for CSWs along the escarpment (Gill, 1982) by taking

$$\psi_n = H_n^{1/2}\varphi_n(x)\exp i(ly - \omega t) \tag{4}$$

where l is the real wave number and ω is the real frequency. In region 2 (away from the Norwegian coast; see comments at the end of the Section), the governing equations (2) and (3) reduce to

$$\varphi_2'' + \kappa^2\varphi_2 = 0 \tag{5}$$

where the prime denotes derivation with respect to x, and

$$\kappa^2 = 2fbl/\omega - b^2 - l^2 \tag{6}$$

We thus have a solution of the form

$$\varphi_2 = G_2 \sin \kappa x + L_2 \cos \kappa x \tag{7}$$

where κ can be imaginary for certain values of l; see Buchwald and Adams (1968) and DWD.

In the flat bottom regions 1 and 3, equations (2)–(4) reduce to

$$\varphi_{1,3}'' - l^2\varphi_{1,3} = 0 \tag{8}$$

We assume zero normal fluxes at $x = -D_1$, and $x = D_3$. Thus, we find

$$\varphi_1 = G_1 \sinh l(x + D_1) \tag{9}$$

$$\varphi_3 = G_3 \sinh l(x - D_3) \tag{10}$$

Furthermore, the volume fluxes and the pressure (here surface elevation) must be continuous at $x = 0$. This leads to

$$G_3 = -L_2/\sinh lD_3 \tag{11}$$

$$G_2 = -L_2/q \tag{12}$$

Here

$$q = \kappa T/(l - bT) \tag{13}$$

where $T = \tanh lD_3$.

From the continuity of volume fluxes at $x = -B$, we have

$$G_1 = -G_2(\sin \kappa B + q \cos \kappa B) / \sinh l(D_1 - B) \tag{14}$$

Finally, continuity of pressure at $x = -B$ yields the transcendental equation for the determination of κ:

$$\tan \kappa B = -[q + P(\kappa + bq)] / [1 + P(b - \kappa q)] \tag{15}$$

where

$$P = (\tanh l(D_1 - B)) / l \tag{16}$$

For the trivial case $D_1 = B$, $D_3 = 0$ (channel with impermeable walls and exponential bottom), we find from (15) that $\tan(kB) = 0$, i.e.

$$\kappa = m\pi/B, \quad m = 1, 2, 3 \tag{17}$$

For a coastal wall at $x = 0$ and an infinitely wide, deep ocean, i.e. $D_1 \to \infty$, $D_3 = 0$, (15) reduces to

$$\tan \kappa B = -\kappa / (l + b) \tag{18}$$

(Buchwald and Adams, 1968). Finally, for an infinitely wide, deep ocean and an infinitely wide inner shelf ($D_1 \to \infty$, $D_3 \to \infty$), we again recover the result by Buchwald and Adams:

$$\tan \kappa B = 2\kappa l \,/\, \left(b^2 + \kappa^2 - l^2\right) \tag{19}$$

In our problem, we consider CSWs with the diurnal frequency $\omega = \omega_{K1}$. Then using $b = 1.117 \times 10^{-5}$ m^{-1}, $B = 100$ km, and $f = 1.3 \times 10^{-4}$ s^{-1}, as in DWD, we have plotted $(\kappa B)^2$ as function of lB from (6) in Fig. 5.

We note immediately from the figure that the transverse wave number κ becomes imaginary for small values of l, i.e. long waves. As seen from Fig. 2, small values of l yields $d\omega/dl > 0$, corresponding to energy transport towards Spitsbergen. Introducing $\kappa = -ip$, and taking $D_1 \to \infty$, $D_3 = 1200$ km, we find from (15) that $p = -9.92 \times 10^{-6}$ m^{-1} for $l = 6.716 \times 10^{-7}$ m^{-1}, which constitutes the only possible mode for $\omega = \omega_{K_1}$, as seen from DWD, their Fig. 4.

Defining $Q = H_0^{1/2}G_2$ in (7), the stream function in the three regions can be written

$$\psi_1 = -Q \exp(bB)[(\sin \kappa B + q \cos \kappa B)\sinh l(x + D_1)/\sinh l(D_1 - B)]\exp i\theta, \quad -D_1 \le x \le -B, \tag{20}$$

$$\psi_2 = Q \exp(-bx)[\sin \kappa x - q \cos \kappa x]\exp i\theta, \quad -B \le x \le 0, \tag{21}$$

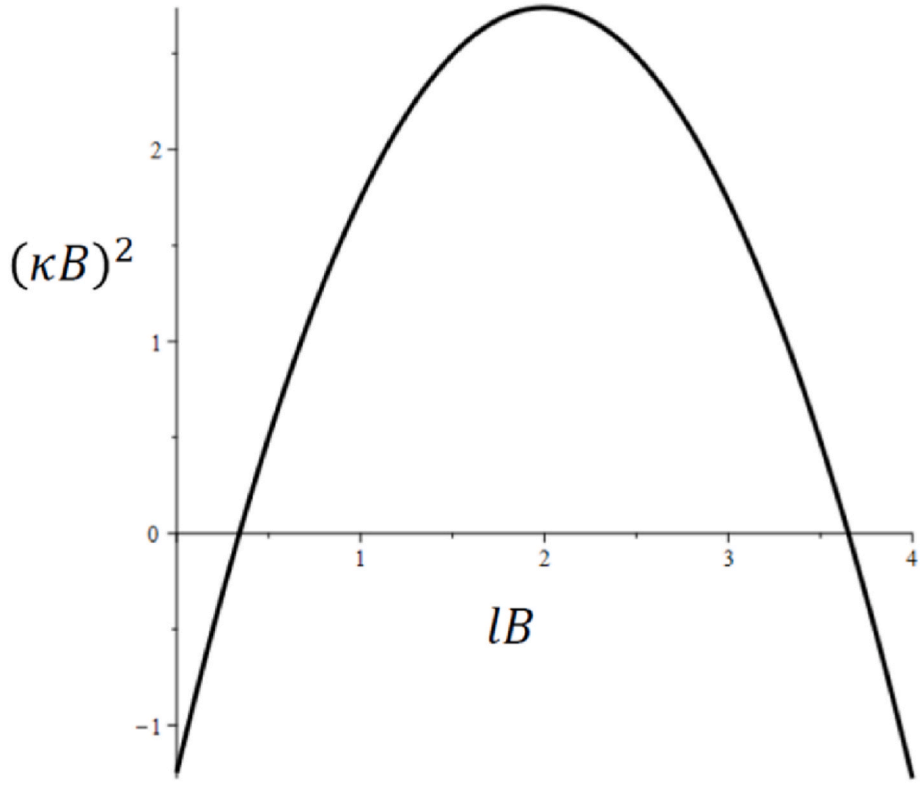

Fig. 5. Non-dimensional squared wave number $(\kappa B)^2$ vs. lB for diurnal CSWs along the escarpment towards Spitsbergen.

$$\psi_3 = Qq[\sinh l(x - D_3)/\sinh lD_3]\exp i\theta, \quad 0 \le x \le D_3, \tag{22}$$

where $\theta = ly - \omega t$ is the phase function. With reference to the model limitations depicted in Fig. 3, we emphasize that the solutions (20)–(22) are valid for $y > L_R$, where L_R is of the order of the barotropic Rossby radius.

Finally, for the surface elevation in the considered domain, we obtain from (2)-(3) that

$$\eta_n = [\omega\psi_{nx} + fl\psi_n] / (gH_n l) = \zeta_n(x)\exp i\theta \tag{23}$$

Here $\zeta_1, \zeta_2, \zeta_3$ are obtained by inserting from (20)-(22).

3. Energy fluxes

3.1. Continental shelf waves

The mean wave energy per unit density and unit area for CSWs can be written

$$\overline{e} = \frac{1}{2}\left(\int_{-H}^{0}\left(\overline{u^2} + \overline{v^2} + \overline{w^2}\right)dz + g\overline{\eta^2}\right) \tag{24}$$

where the over-bar symbolizes average over the wave cycle. We now utilize that the waves are long. Then we can neglect the contribution from the vertical velocity w in the kinetic energy part. Furthermore, for the parameters used here, we find that the ratio of the potential energy to the kinetic energy in (24) varies from 5×10^{-3} to 1×10^{-1} over the shelf. Hence, we neglect the small contribution from the potential energy in (24). Then, for barotropic flow, we have approximately that

$$\overline{e} = \frac{1}{2}H\left(\overline{u^2} + \overline{v^2}\right) \tag{25}$$

The mean energy E per unit density and unit length along the escarpment can thus be written

$$E = \int_{-D_1}^{-B}\overline{e}_1 dx + \int_{-B}^{0}\overline{e}_2 dx + \int_{0}^{D_3}\overline{e}_3 dx = E_1 + E_2 + E_3 \tag{26}$$

Since $u = -\psi_y/H$, and $v = \psi_x/H$, the mean energy can be obtained from the real parts of (20)-(22). By trivial calculations, we find

$$\overline{e}_1 = \left(l^2Q^2 / 4H_0\right)\left[(\sinh pB + \widehat{q}\cosh pB)^2 / \sinh^2 l(D_1 - B)\right]\cosh 2l(x + D_1), \tag{27}$$

where $\widehat{q} = pT/(l - bT)$. Furthermore,

$$\overline{e}_2 = (Q^2/(4H_0))\left[l^2\{\sinh px - \widehat{q}\cosh px\}^2 + \{-(b + p\widehat{q})\sinh px + (p + b\widehat{q})\cosh px\}^2\right] \tag{28}$$

and

$$\overline{e}_3 = \left[l^2Q^2\widehat{q}^2 / \left(4H_0\sinh^2 lD_3\right)\right]\cosh 2l(x - D_3) \tag{29}$$

The energy flux F_{CSW} in the CSW can then be written

$$F_{CSW} = c_g(E_1 + E_2 + E_3) \tag{30}$$

where c_g is the group velocity. Here E_1, E_2, E_3 are easily obtained from (26)-(29). Using the parameters in this study, we find from (30) that

$$F_{CSW} = rQ^2 \tag{31}$$

where $r = 9.71 \times 10^{-8}\ \mathrm{m^{-1}s^{-1}}$. Below, Q will be determined from the energy flux balance of the wave motion.

3.2. Incident and transmitted Kelvin waves

With reference to the diagram in Fig. 3, the incident tidal K_1 signal is a coastal Kelvin wave, trapped within the barotropic Rossby radius of deformation. For a fluid column, the mean kinetic and the mean potential energy in Kelvin waves are equal. By integrating from the coast to

infinity in an ocean of constant depth H, the total mean energy E_k (subscript k for Kelvin) per unit density and unit length along the coast is (Gill, 1982),

$$E_k = g^{3/2}H^{1/2}A^2 \,/\, (4f) \tag{32}$$

where A is the amplitude at the coast. The group velocity in shallow-water Kelvin waves is $c_g = (gH)^{1/2}$. Hence, the energy flux F can be written as

$$F = c_g E_k = g^2 H A^2 \,/\, (4f) \tag{33}$$

The fluxes (30) and (33) will now be used to estimate the energy balance in this problem.

3.3. Energy flux balance

We write the Kelvin wave fluxes west and east of the escarpment as F_1 and F_3, respectively, and neglect the energy loss to bottom friction in this problem. The energy flux balance for the wave motion then becomes

$$F_{CSW} = F_1 - F_3 \tag{34}$$

where F_{CSW} is given by (30), and F_1, F_3 by (33). This situation is sketched in Fig. 6.

The ratios of the energy fluxes relative to that of the incident wave, may be written

$$R = F_3/F_1 \tag{35}$$

$$R_{CSW} = F_{CSW}/F_1 = 1 - R \tag{36}$$

Obviously, if no CSW is possible along the escarpment (i.e. frequencies larger than f), (35) implies that $R = 1$, and hence from (33),

$$A_3 \,/\, A_1 = (H_1/H_3)^{1/2} \tag{37}$$

We note that for the depth ratio in Fig. 4, this would mean for the upper limit that $A_3/A_1 = 3.1$.

From the TPXO analysis depicted in Fig. 1, we note that the K_1 amplitudes at the coast, both east and west of the escarpment towards Spitsbergen, is typically of the order 0.1 m. This fits well with values from the Tide Tables for the Norwegian coast and Svalbard (Det Norske Kartverk, 2021). From a coastal station west of the escarpment (Sandnessjøen, 66°01′ N, 12°39′ E) we find that $A_1 = 0.09$ m for the tidal K_1 component. At a station east of the escarpment (Vardø, 70°20′ N, 31°06′ E) we have $A_3 = 0.12$ m for this component. Hence, for estimating the energy flux towards Spitsbergen, we may assume that $A_3/A_1 = 1.3$.

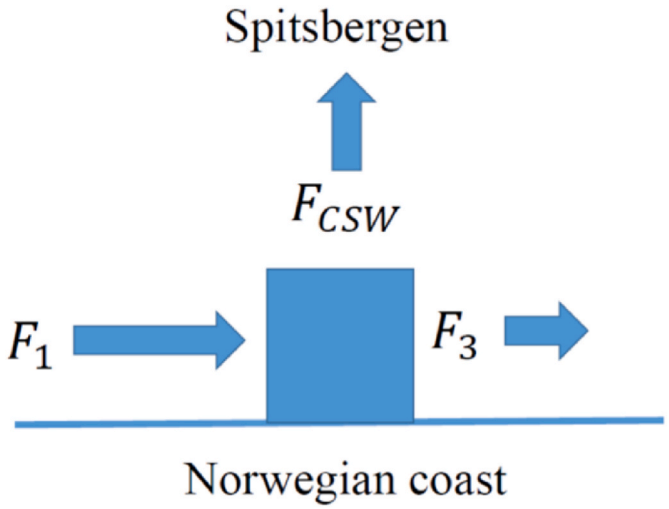

Fig. 6. Schematic diagram of wave energy fluxes.

Using this value, we find from (35) that $R = 0.18$, and hence, from (36), $R_{CSW} = 0.82$. This means that about eighty percent of the incident diurnal Kelvin energy flux continues in the form of CSWs along the escarpment towards Spitsbergen, and only about twenty percent is transmitted into the Barents Sea as coastally trapped Kelvin waves.

From (33) and the balance equation (34), we then obtain

$$Q^2 = g^2\left(H_1A_1^2 - H_3A_3^2\right) \,/\, (4rf) \tag{38}$$

which relates Q in the CSW solution to the Kelvin wave amplitudes A_1 (west) and A_3 (east) of the escarpment. As shown in Section 2, the wave number for the diurnal CSW is $l = 6.716 \times 10^{-7}$ m^{-1}. From Fig. 2 we note that these long waves are practically non-dispersive, so here $c_g = \omega_{K_1}/l$. Inserting for the parameters above, we find from (38) that $Q = 5.95 \times 10^6$ m^3 s^{-1}. Using this value in (23), we have plotted the surface elevation amplitude ζ of the CSW in Fig. 7.

In Fig. 7 we have only displayed ζ values for smaller part of regions (1) (dashed) and (3) (dash-dot) in order to have a readable variation of ζ over the narrow escarpment. The variation in the deep and shallow regions resembles very much that of a double Kelvin wave (Longuet-Higgins 1968).

We find from the Tidal Tables that the K_1 surface amplitude in Ny-Ålesund on the west coast of Spitsbergen, bordering the escarpment, is 0.064 m. Accordingly, the result for the surface elevation displayed in Fig. 7 for our highly idealized geometry, captures the correct order of magnitude of the observed values.

In the next Section, we perform numerical simulations for the same idealized escarpment profile. This may provide a check of the basic physical assumptions as well as the analytical results presented in the previous sections.

4. Numerical simulations

Numerical simulations were carried out with the ROMS ocean model (Shchepetkin and McWilliams, 2005; Haidvogel and Coauthors, 2008) configured in 2D mode, i.e. for a constant-density ocean. An idealized rectangular domain of size 8000 km × 8000 km, using grid spacing of 10 km, was set up with bottom topography as in (1) and Fig. 4. The model was forced with an imposed Kelvin wave signal for the sea surface height (SSH) and velocity variations at the western boundary given by

$$\eta_1 = A_1 \exp(-y/a_1)\sin \omega t \tag{39}$$

$$u_1 = (gA_1/c_1)\exp(-y/a_1)\sin \omega t \tag{40}$$

$$v_1 = 0 \tag{41}$$

where A_1 is the wave amplitude at the southern wall, $c_1 = (gH_1)^{1/2}$ is the phase speed in the deep ocean and $a_1 = c_1/f$ is the external Rossby radius. The incoming signal was provided at the western boundary using the Chapman (1985) and Flather (1976) boundary conditions, which let deviations from the prescribed signal propagate out of the domain with the shallow-water phase speed. For illustrative purposes, the incident wave amplitude was taken to be 1 m for the M_2 wave and 0.1 m for the K_1 wave. The model also used Chapman and Flather conditions at the northern and eastern boundaries, allowing radiation of deviations from zero SSH and velocities. To damp out any reflections from the northern boundary, we also introduced a 1000 km wide sponge region there where harmonic viscosity was ramped up from zero in the interior to 5000 m^2 s^{-1} at the boundary. Finally, an impermeable wall condition was set along the southern boundary at $y = 0$. Model runs presented here contained no advection of momentum and used a quadratic bottom drag coefficient $c_D = 2 \times 10^{-3}$.

Fig. 8 shows snapshots of SSH for two different runs that have been forced with M_2 and K_1 components, respectively. Both simulations clearly reveal the Kelvin wave signal along the southern boundary. Offshore e-folding scales and wavelengths are reduced as the waves

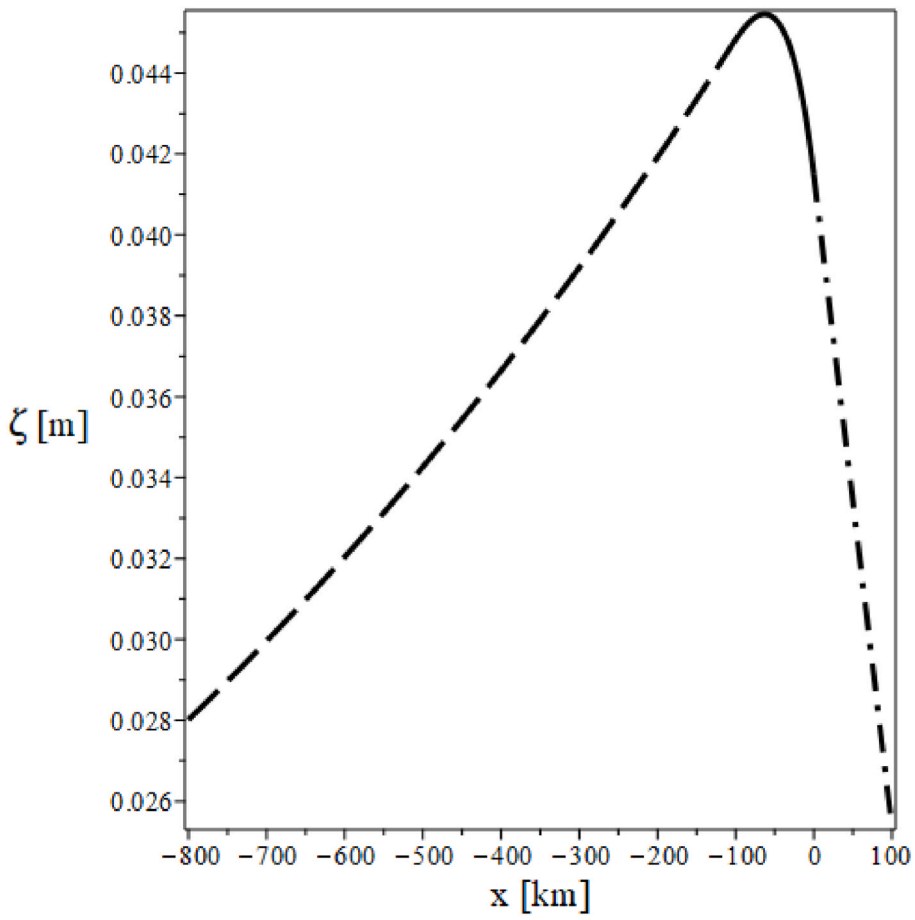

Fig. 7. Surface elevation amplitude $\zeta(x)$ of the CSW from the deep region (1) to the shallow region (3). The solid part of the curve shows the variation across the escarpment.

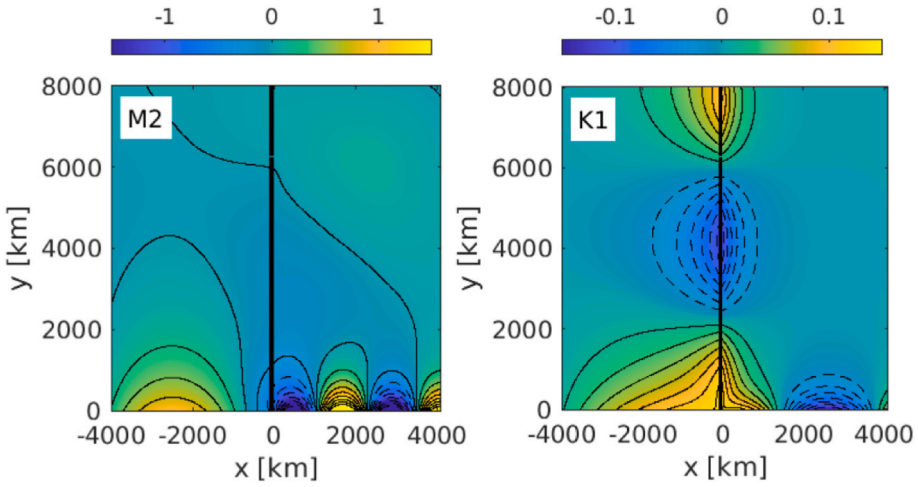

Fig. 8. Snapshot of SSH amplitude (in meters) of the M_2 (left) and K_1 (right) tide for the idealized model simulation. Contour lines are drawn every 0.25 m. Dashed lines represent negative values.

travel from deep to shallow waters, as expected from theory. In particular, for Kelvin waves of given frequency, the ratio of the wavelengths in the deep and shallow regions is here $(H_1/H_3)^{1/2} = 3$, which is seen to fit well for M_2 in Fig. 8 (left panel).

Most importantly, however, we note from Fig. 8 that the simulations support our hypothesis that the diurnal tide can propagate as a CSW northward along the escarpment, whereas the semi-diurnal tide cannot. From the figure, we observe that the wavelength of the CSW in the numerical run is about 7500 km, while the analytical value was $\lambda = 2\pi/l \approx 9400$ km. This is a reasonably good fit, taking into consideration the differences between the analytical and numerical models; see the discussion in Sec. 5.

Fig. 9 shows the SSH amplitude (RMS times the square root of two) from the two runs, calculated after the Kelvin wave front has reached the

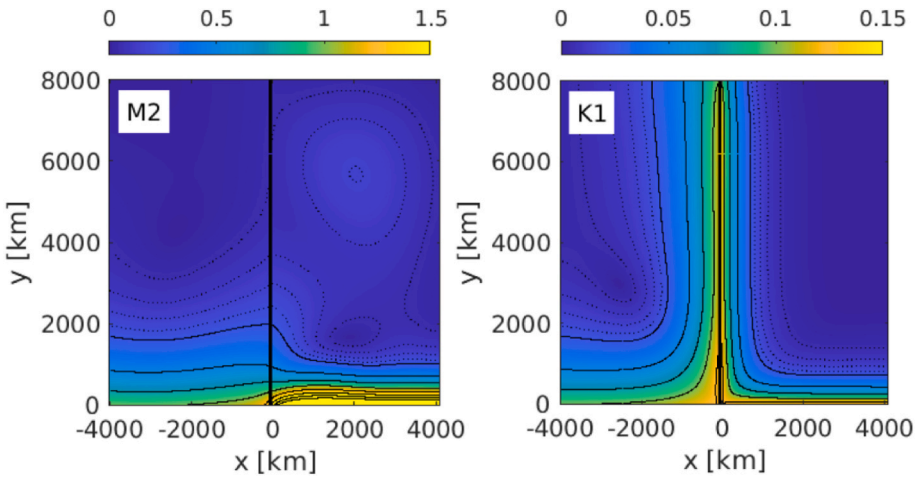

Fig. 9. The SSH amplitude (in meters) of the M_2 (left) and K_1 (right) tide for the idealized model simulation. Contour lines are drawn every 0.05 m up to 0.2 m and then every 0.25 m.

eastern boundary. The difference in offshore e-folding scales between deep and shallow regions is now even more clearly seen, and we can also discern the expected increase in amplitude as the Kelvin waves traverse the escarpment, especially for the M_2 tide. Some energy of this component appears to radiate as Poincaré waves into the Barents Sea model interior, but the bulk traverses the escarpment along the southern wall. The amplitude increase over the escarpment is considerably lower for the K_1 tide, and the plot clearly reveals the northward propagation of diurnal energy along the escarpment.

Fig. 10 depicts the wave amplitude of the two components along the southern boundary ($y = 0$). Recall that, if the Kelvin wave energy flux were conserved (no generation of Poincaré waves or CSWs, and no frictional effects), (37) would dictate the amplitude change. As mentioned before, with $H_1 = 2800$ m and $H_3 = 300$ m, we expect an upper limit to the sea surface height ratio of $A_3/A_1 = 3.1$.

We note that the modeled ratio for the M_2 component (left panel) is about 2.7, which is somewhat lower than the upper limit of 3.1. The difference can likely be ascribed to the weak Poincaré signal seen in the numerical runs, as well as to the fact that the simulation has finite bottom friction. In contrast, the modeled sea surface height ratio for the K_1 component (right panel) is about 1.4, more than fifty percent lower than the theoretical upper bound for conservation of Kelvin wave energy flux. Friction acts approximately in the same way in the two simulations, so the enhanced energy loss for this component is predominately due to CSW radiation along the escarpment. Previously, in Sec. 4, the amplitude ratio was assessed as 1.3 from the Tidal Tables, which is very close to our numerical result. Hence, also the model results support the conclusion that about 80 percent of the incident K_1 energy is lost from the Kelvin wave to the CSW.

Finally, in Fig. 11 we have plotted the wave amplitude along and across the escarpment. The left panel shows the amplitude along the escarpment at the shelf break $x = 0$ and at the bottom of the escarpment ($x = -100$ km). The structure is rather intricate, with what is likely a combined signature of the Kelvin wave and the kinematic boundary condition for the CSW near the southern coast. A few deformation radii away from the coast the amplitude, however, takes on a value somewhat above 0.1 m. Finally, near the northern boundary, there is a drop in amplitude, which we believe is an adjustment to the open boundary condition and the 1000 km-wide sponge zone in this region.

The right panel of the figure shows the amplitude along a transect which crosses the escarpment at $y = 4000$ km. The model response over the escarpment is qualitatively similar to the analytical calculations depicted in Fig. 7, though we notice that the maximum amplitude in the model is 0.11 m, which is more than twice that of the analytical result. Again, such deviations can probably be attributed to differences in the analytical and numerical modeling conditions; see the discussion below.

5. Summary and concluding remarks

The TPXO (v9) tidal inversion analysis of the sea surface height amplitude by Egbert and Erofeeva (2002) shows considerable energy on the tidal K_1 diurnal frequency off the Norwegian coast and along the escarpment towards Spitsbergen. To investigate this problem in more detail, we perform analytical calculations and numerical modeling with

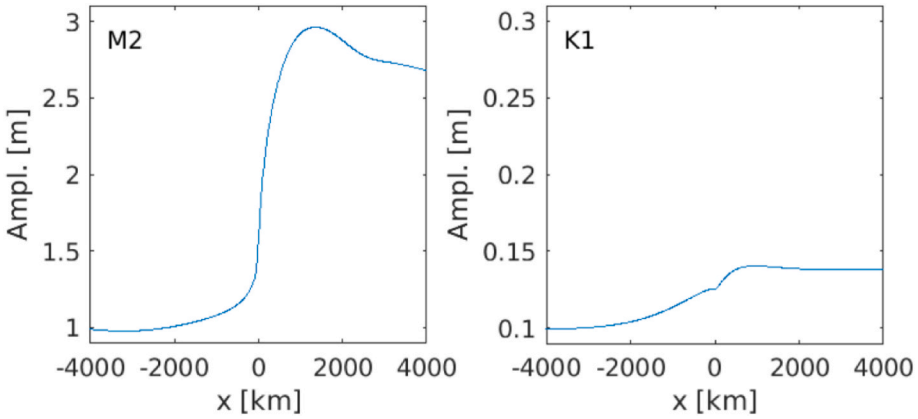

Fig. 10. The SSH amplitude of the M_2 (left) and K_1 (right) tide along the southern wall. Incident wave amplitude is 1 m for M_2 and 0.1 m for K_1.

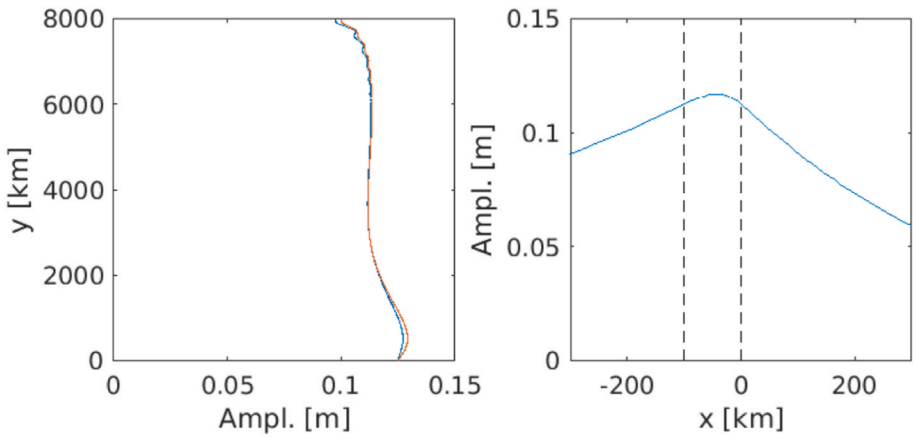

Fig. 11. Left panel: Surface amplitude of the K_1 tide along the escarpment at $x = 0$ (blue) and $x = -100$ km (red). Right panel: Surface amplitude of the K_1 tide across the escarpment at $y = 4000$ km.

an idealized bottom topography and coastal geometry to calculate the energy flux in continental shelf waves (CSWs) towards Spitsbergen. The CSWs are caused by sub-inertial Kelvin wave motion along the west coast of Norway traversing the steep bottom escarpment in the Barents Sea Opening. Analytical calculations with K_1 amplitudes from the Tidal Tables as well as numerical simulations indicate that about eighty percent of the incident diurnal Kelvin wave energy flux outside west Norway continues towards Spitsbergen in the form of CSWs, and only twenty percent of the energy is transmitted into the Barents Sea by the coastal Kelvin K_1 wave.

We find excellent qualitative agreement between the numerical model and analytical results. However, there are also some differences, most notably the CSW SSH amplitude over the escarpment. One thing to note in this respect is that the analytical analysis of the CSWs assumes freely propagating waves along an infinitely long escarpment in the y-direction. The numerical simulations, on the other hand, have a wall in the south. Hence, in the full problem, there is a zone near the southern wall where the CSW dynamics needs to adjust to the zero normal flow condition and the Kelvin wave forcing; with the latter extending typically one to two Rossby radii off the coast. Finally, the analytical treatment considered a Barents Sea of finite extent, whereas the numerical model used a periodic domain in the x-direction. Therefore, the similarity of the two analyses should be viewed in a qualitative sense, and a more detailed treatment will be left for a future study. However, the physics of this problem is quite clear: The energy of the Kelvin K_1 tide along the coast of Norway is largely diverted towards Spitsbergen in the form of CSWs.

Declaration of competing interest

The authors declare that they have no known competing financial interests or personal relationships that could have appeared to influence the work reported in this paper.

Acknowledgements

The authors gratefully acknowledge support from the Research Council of Norway through Grants 276730 (Nansen Legacy) and 314826 (TopArctic).

References

Buchwald, V.T., Adams, J.K., 1968. The propagation of continental shelf waves. Proc. Roy. Soc. Lond. 305, 235–250.
Buchwald, V.T., Kachoyan, B.J., 1987. Shelf waves generated by a coastal flux. Aust. J. Mar. Freshw. Res. 38, 429–437.
Cartwright, D.E., 1969. Extraordinary tidal currents near St. Kilda. Nature 223, 928–932.
Chapman, D.C., 1985. Numerical treatment of cross-shelf open boundaries in a barotropic coastal ocean model. J. Phys. Oceanogr. 15, 1060–1075.
Det Norske Kartverk, 2021. Tide Tables for the Norwegian Coast and Svalbard, 84th Edition.
Drivdal, M., Weber, J.E., Debernard, J.B., 2016. Dispersion relation for continental shelf waves when the shallow shelf part has an arbitrary width: Application to the shelf west of Norway. J. Phys. Oceanogr. 46, 537–549.
Egbert, G.D., Erofeeva, S.Y., 2002. Efficient inverse modeling of barotropic ocean tides. J. Atmos. Ocean. Technol. 19, 183–204.
Foreman, M.G.G., Thomson, R.E., 1997. Three-dimensional model simulations of tides and buoyancy currents along the west coast of vancouver island. J. Phys. Oceanogr. 27, 1300–1325.
Flather, R.A., 1976. A tidal model of the northwest European continental shelf. Mem. Soc. Roy. Sci. Liege 10, 141–164.
Gill, A.E., Schumann, E.H., 1974. The generation of long shelf waves by the wind. J. Phys. Oceanogr. 4, 83–90.
Gill, A.E., 1982. Atmosphere-Ocean Dynamics. In: Int. Geophys. Ser., vol. 30. Academic Press, p. 662.
Haidvogel, D., Coauthors, 2008. Ocean forecasting in terrain-following coordinates: formulation and skill assessment of the regional ocean modeling system. J. Comput. Phys. 227, 3595–3624.
Huthnance, J.M., 1975. On trapped waves over a continental shelf. J. Fluid Mech. 69, 689–704.
Lam, F.-P.A., 1999. Shelf waves with diurnal tidal frequency at the Greenland shelf edge. Deep-Sea Res. I 46, 895–923.
Longuet-Higgins, M.S., 1965. Some dynamical aspects of ocean currents. Quart. J. R. Met. Soc. 91, 425–451.
Longuet-Higgins, M.S., 1968. Double Kelvin waves with continuous depth profiles. J. Fluid Mech. 34, 49–80.
Middleton, J.F., 1988. Long shelf waves generated by a coastal flux. J. Geophys. Res. 93 (10), 724-10,730.
Moe, H., Ommundsen, A., Gjevik, B., 2002. A high resolution tidal model for the area around. The Lofoten Islands. Continent. Shelf Res. 22, 485–504.
Morrow, R.A., Jones, I.S.F., Smith, R.L., Stabeno, P.J., 1990. Bass Strait forcing of coastal trapped waves: ACE revisited. J. Phys. Oceanogr. 20, 1528–1538.
Shchepetkin, A.F., McWilliams, J.C., 2005. The regional oceanic modeling system (ROMS): a topography-following-coordinate oceanic model. Ocean Model. 9, 347–404.
Weber, J.E., Børve, E., 2021. Diurnal continental shelf waves with a permeable boundary: Application to the shelf northwest of Norway. Eur. J. Mech. B Fluid 89, 64–71.
Weber, J.E., Børve, E., 2022. On group velocity and spatial damping of diurnal continental shelf waves. Continent. Shelf Res. 232, 104630.